

Collisions between rare-gas atoms at low-keV energies. II. Asymmetric collision systems: He-Ne, -Ar, -Kr, -Xe

J. C. Brenot, D. Dhuicq, J. P. Gauyacq, J. Pommier, V. Sidis, M. Barat, and E. Pollack*

Laboratoire de Collisions Atomiques† Bâtiment 220, Université Paris-Sud, 91405 Orsay, France

(Received 26 December 1974)

Elastic and inelastic collisions in the asymmetric He- X ($X = \text{Ne, Ar, Kr, Xe}$) systems are studied at low-keV energies (0.8–3.0 keV). The experimental method involves energy-loss measurements on the scattered particles using either a time-of-flight technique (for neutrals) or electrostatic energy analysis (for ions). Differential cross sections are reported and the results interpreted in a quasimolecular treatment of the collision. Of particular significance is the very low excitation and ionization of the helium projectile relative to excitation of the target. An understanding of this requires a modification of the usual diabatic correlation rules, and implies the promotion of the outer filled molecular orbital. Predictions made from the modified correlation diagram, and calculated potential-energy curves are found to agree with the experimental results.

I. INTRODUCTION

In a previous paper¹ (hereafter referred to as I) we reported on symmetric rare-gas-rare-gas collisions. These earlier studies were discussed in a quasimolecular framework, and predictions of the promotion model² together with *ab initio* molecular calculations were found to explain the experimental results. All excitations in the symmetric rare-gas systems occur either directly or indirectly via the promotion of the outer filled MO (molecular orbital) from which one or two σ electrons can make transitions to empty excited MO's.

The present paper extends the study to helium-rare-gas collisions in order to assess the effect of the strong asymmetry in the collision systems. A special feature of these systems is the matching of the K -shell energy of helium with that of the L, M, \dots shells of the partner. In particular, it is important to know whether the excitation takes place in both partners or selectively in one of them. For this purpose one can use the predictions of the asymmetric diabatic correlation diagrams which have thus far proved to be very powerful in dealing with inner-shell excitations.³

The experimental methods involve energy analysis of the scattered particles using both a time-of-flight technique (for neutrals^{1,4}) and electrostatic energy analysis (for ions). Differential cross sections, over a range of beam energies and scattering angles, are obtained from the relative intensity of the peaks in the energy-loss spectra. Details of the experimental procedure were given in I and are not repeated here.

In the first section the energy-loss spectra and their main features are presented for all the systems. Cross sections are reported in Sec. II, and all the experimental results are discussed in Sec.

III using a quasimolecular framework. As in I, the predictions made from the diabatic correlation diagrams together with the calculated potential energy curves (for the He-Ne and He-Ar cases) are compared with the experimental results.

II. ENERGY-LOSS SPECTRA

A. He-Ne

1. Neutrals

Typical energy-loss spectra are shown in Fig. 1. Generally, three peaks (or groups of peaks) are seen and correspond to zero-, one-, or two-electron excitations. Peak A in the spectra represents elastically scattered particles. Peak B , associated with single-electron excitation, generally displays three components: $B_1, B_2,$ and B_3 . The peak B_1 , corresponding to $\text{Ne}(2p^5 3s)^1P$, is dominant for low-energy collisions (0.75 and 1 keV) and at larger angles for higher energies. Evidence for the excitation of $\text{Ne}(2p^5 3p)$, peak B_3 , is found, especially at low energy, when sufficiently good energy resolution is obtained. The B_2 structure may correspond to high-lying singly excited states of Ne. It can be seen that this peak, which is dominant at small angles and for moderate and high-energy collisions, is centered on $\text{Ne}(2p^5 4s)$ and/or $(2p^5 3d)$ —a feature which will be found again in the other He-rare-gas combinations. However, contributions from $\text{He}(2^1S)$ and from higher excited He levels cannot be excluded since they lie in the same energy range. At larger angles, peak B_2 is followed by a tail attributable to Ne ionization (confirmed by the Ne-He ionization spectra below).

In the third group of peaks C , simultaneous excitation of He and Ne into

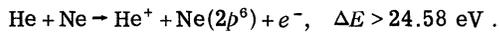
$\text{He}(1s2s) + \text{Ne}(2p^5 3s)$, $\Delta E = 36.5$ and/or 37.5 eV,

readily accounts for the C_1 component which is dominant at small values of $\tau = E\theta$ [(beam energy) \times (scattering angle)].

At larger τ the second feature C_2 , lying at about 40–44 eV, can be explained by simultaneous single-electron excitation of both atoms to higher states. Although autoionizing states of Ne lie in this energy region (see Fig. 1) the absence of the corresponding peaks in the ejected-electron spectra⁵ would seem to rule out this possibility.

2. Ions

Ionizing collisions may of course result in either He^+ or Ne^+ ions. With He incident on a Ne target, He^+ ions are studied (a Ne beam colliding with a He target permits the study of the Ne^+ product). Figures 2(a) and 2(b) show typical examples of the He^+ spectra. Two peaks are generally present: peak B' corresponds to He ionization leaving the Ne in the ground state,



We may note that the position of the maximum of B' is shifted by a few eV with respect to the energy threshold and corresponds to electrons ejected with nonzero kinetic energy. This feature has already been discussed for He-He collisions.⁶ The smooth tail of B' corresponds to a continuous dis-

tribution of ejected-electron energies.⁵

As in the neutral spectra, peak C'_1 [Fig. 2(b)] accounts for two-electron excitation leading to $\text{He} + \text{Ne} \rightarrow \text{He}^+(1s) + \text{Ne}(2p^5nl)$, $41 \text{ eV} < \Delta E < 46 \text{ eV}$.

A more precise assignment cannot be given.

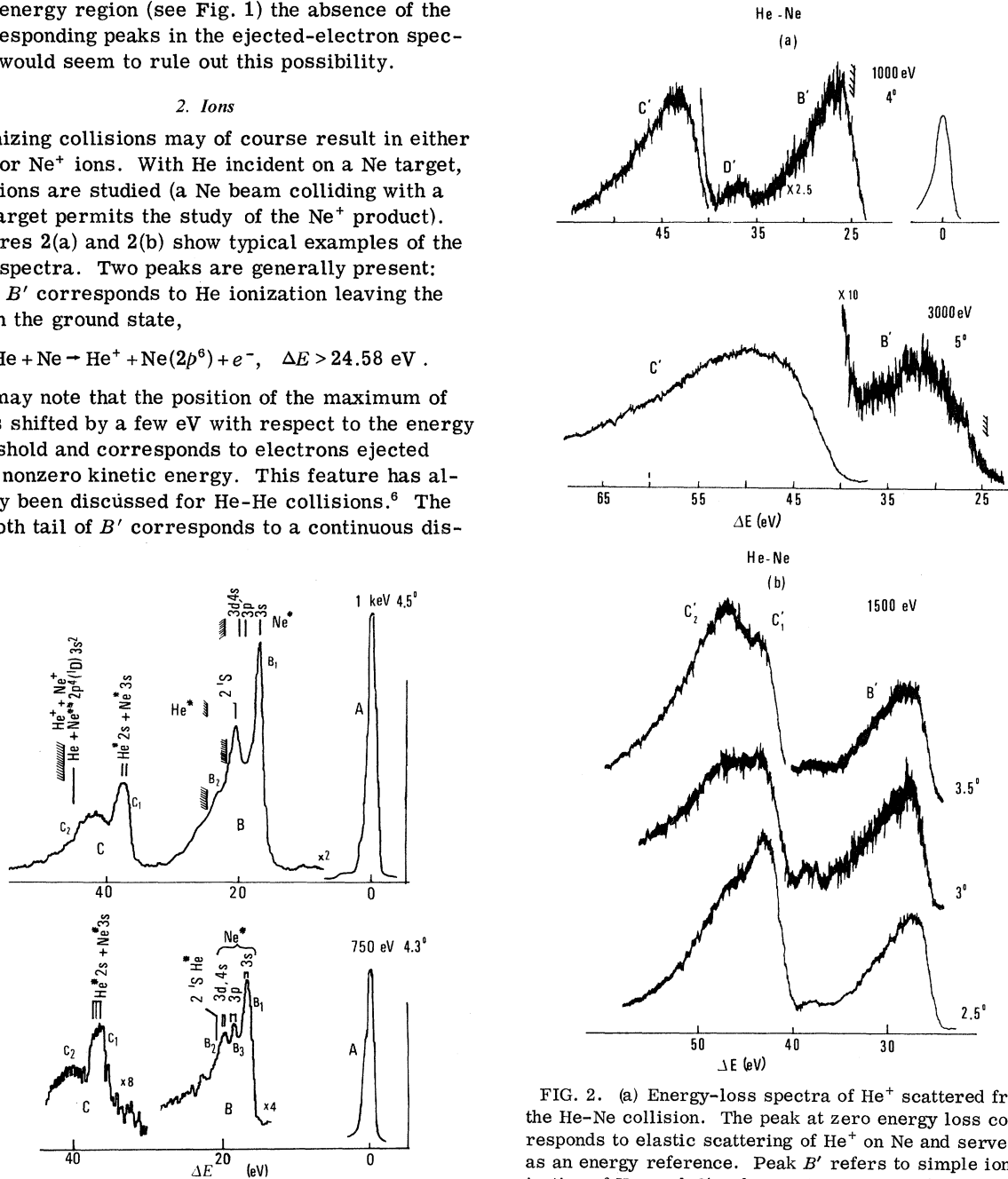
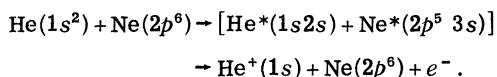


FIG. 1. Energy-loss spectra of neutral He scattered from the He-Ne collision. Peak A refers to the elastic process, peak B to one-electron excitation, and C to two-electron excitation.

FIG. 2. (a) Energy-loss spectra of He^+ scattered from the He-Ne collision. The peak at zero energy loss corresponds to elastic scattering of He^+ on Ne and serves as an energy reference. Peak B' refers to simple ionization of He, and C' refers to ionization with simultaneous excitation of Ne. D' is the peak for "inverse Penning" discussed in the text. (b) These spectra show the evolution of the C'_1 and C'_2 structures as a function of angle.

For violent collisions a second feature C'_2 appears at $\Delta E > 45$ eV [Fig. 2(b)]. For $\tau > 10$ keV deg it dominates the ion spectra and spreads out considerably up to a 70-eV energy loss [Fig. 2(a)]. We attribute C'_2 to simultaneous ionization of both particles with the ejection of energetic electrons (see Sec. III).

In addition to the dominant B' and C' peaks, a small structure (D') is clearly seen at $\Delta E \sim 37$ eV and can be ascribed to a "molecular autoionization" (also called "inverse Penning ionization"⁵) proceeding as



This assignment is consistent with the strong peak, observed in the neutral spectra, for the $\text{He}(1s 2s) + \text{Ne}(2p^5 3s)$ simultaneous excitation.

Ejected electrons coming from inverse Penning [$\text{He}(^3S) + \text{Ne}(^3P)$] ionization would have energies of 12 or 15 eV according to whether the decay takes place in the He^+ or Ne^+ continua. For the $\text{He}^*(2^1S) + \text{Ne}^*(3^1P)$ inverse Penning ionization the corresponding electron energies should lie at 13 and 16 eV, respectively. In their experiment Gerber *et al.*⁵ do not see any electron peak below 16 eV and reject this process as responsible for autoionization. The absence of the 12-eV peak in the ejected-electron spectra of Gerber *et al.*⁵ is consistent with the weak formation of He^+ ions as seen in our experiments. If their dominant 16-eV peak accounts for the $\text{He}(2^1S) + \text{Ne}(3^1P)$ "inverse Penning ionization," a 15-eV peak should *a priori* also be observed except if the autoionization probability favors the 16-eV peak. Although this reassignment would nicely fit the present interpretation (Sec. IV), a definite conclusion requires further investigation.

Figure 3 shows an example of the Ne^+ spectra from the inverse Ne-He collision. Because of the

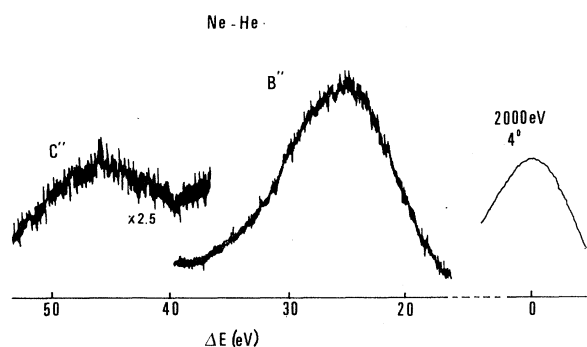


FIG. 3. Energy-loss spectrum of Ne^+ scattered from the Ne-He collision. The same labeling is used as in Fig. 2.

unfavorable mass ratio, the resolution is very poor and only the gross features are seen. The two features B'' and C'' correspond to single Ne ionization and ionization with simultaneous He excitation.

B. He-Ar

1. Neutrals

The energy-loss spectra for He-Ar (Fig. 4) again display three peaks or groups of peaks. It is noteworthy that the peaks labeled B , corresponding to single-electron excitation of Ar, have the same pattern as in the He-Ne case: the first one, B_1 , is, without any doubt, assigned to the first excited Ar level $\text{Ar}^*(3p^5 4s)$; the second one, B_2 , is a result of the excitation of higher states. This peak is centered on $\text{Ar}^*(3p^5 3d)$ and $\text{Ar}^*(3p^5 5s)$. Again the $4p$ states seem rather weakly excited in contrast to the Ar-Ar case.¹

As a striking feature we may note the absence of any significant excitation of the He atom. The data show that He excitation is at least 20 times smaller than Ar excitation. In contrast to the previous He-Ne case, the C_1 peak cannot be accounted for by the simultaneous excitation of both colliding particles and must be attributed to an autoionizing state of Ar. C_1 corresponds to the dominant 12.9-eV line observed by Gerber *et al.*⁵ in the ejected-electron spectra and was tentatively attributed by them to $\text{Ar}^{**}[3p^4(^3P)3d 4s]$. However, using the empirical method proposed by Bolduc⁷ for estimating the autoionizing energy levels in the Ne case, we obtain the following values for the optically forbidden $3p^4 4s^2$ levels:

$$3p^4(^3P)4s^2 \quad (\Delta E \sim 26.5 \text{ eV})$$

$$3p^4(^1D)4s^2 \quad (\Delta E \sim 28.3 \text{ eV})$$

$$3p^4(^1S)4s^2 \quad (\Delta E \sim 30.6 \text{ eV}).$$

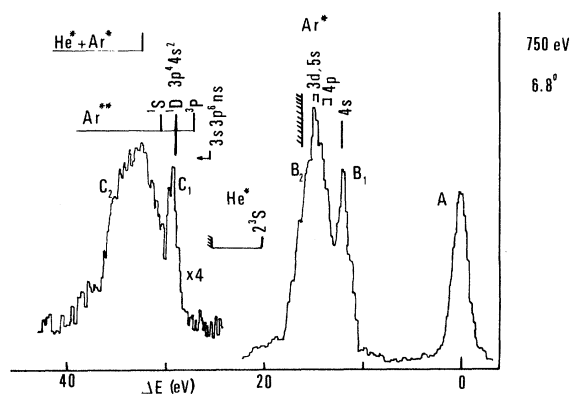
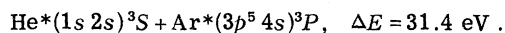


FIG. 4. Energy-loss spectrum of neutral He scattered from the He-Ar collision. The same labeling is used as in Fig. 1.

We believe then, that peak C_1 may result (at least partially) from the $3p^4(^1D)4s^2$ level rather than from the previous assignment⁵: In addition to the theoretical considerations developed in the discussion, this assignment is supported by the similarity observed in the He-Kr collision (see Sec. II C). The weakness of the $3s$ excitation, leading to autoionizing levels Ar ($3s3p^6nl$), is in agreement with the ejected-electron data.⁵

Peak C_2 may be accounted for by excitation of higher lying ($3p^4nl n'l'$) autoionizing levels. However, the simultaneous excitation of both particles may contribute significantly to C_2 since, in particular, this peak is centered on the first excited level of the series $He^* + Ar^*$:



2. Ions

Only the He^+ ions are studied in this very asymmetric system since the unfavorable mass ratio does not permit an investigation of the Ar-He collision with sufficient energy resolution.

Again, two peaks are seen in the He^+ spectra (Fig. 5) corresponding, respectively, to simple He ionization (peak B'), and to ionization with simultaneous Ar excitation (peak C'). It is found that B' is always peaked on the ionization threshold ($\Delta E = 24.5 \text{ eV}$), corresponding to a very low kinetic energy of the ejected electrons. It is also remarkable that the maximum of C' always lies at 36.2 eV, and this accounts without ambiguity for the excitation of $Ar(3p^54s)$ simultaneously with the He ionization. We do not find any evidence for "inverse-Penning"-type ionization processes decaying in the He^+ continuum. An explanation of this will be given in the discussion.

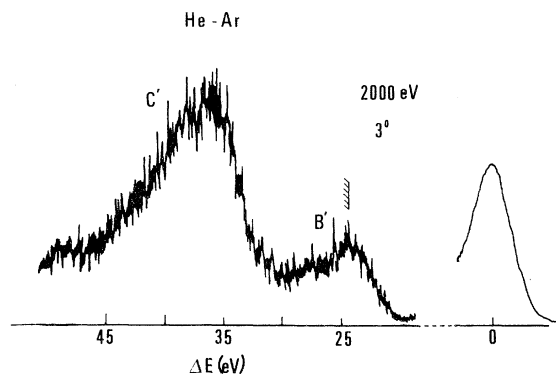


FIG. 5. Energy-loss spectrum of He^+ scattered from the He-Ar collision. The same labeling is used as in Fig. 2.

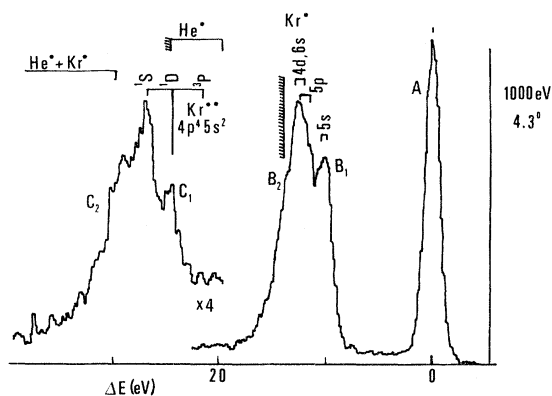


FIG. 6. Energy-loss spectrum of neutral He scattered from the He-Kr collision. The same labeling is used as in Fig. 1.

C. He-Kr and He-Xe

1. Neutrals

The energy-loss spectrum shown in Fig. 6 displays a striking similarity to that obtained in the He-Ar case. Peak B , corresponding to single-electron excitation of Kr, again shows a double structure. B_1 corresponds to $Kr(4p^55s)$ excitation, whereas the dominant B_2 peak is centered on the $6s$ and $4d$ Kr levels. It is also remarkable that there is no significant excitation of the He atom.

The two-electron excitations (peak C) seem to take place almost exclusively in the Kr atom. Peak C_1 can be attributed to $Kr^{**}[4p^4(^1D)5s^2]$, in agreement, in this case, with the assignment proposed by Gerber *et al.*⁵ for the 10.5-eV peak in their

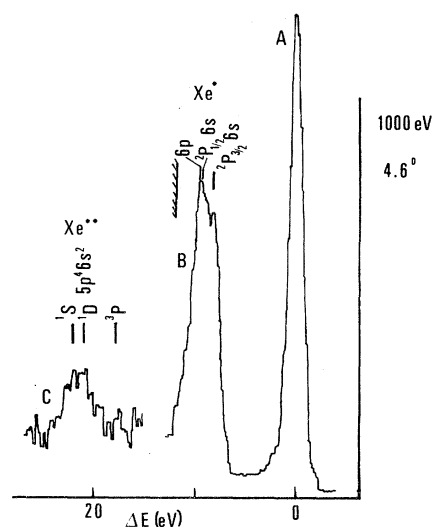


FIG. 7. Energy-loss spectrum of neutral He scattered from the He-Xe collision. The same labeling is used as in Fig. 1.

ejected-electron spectra. The C_2 peak and structure on the high-energy-loss side of C cannot be easily identified; however, it is probably due to $Kr^{**}(4p^4nl n'l')$. Simultaneous excitation (if it occurs) of both particles is seen to be very weak, again in contrast with the He-Ne case.

The energy-loss spectrum obtained in the He-Xe case is displayed in Fig. 7, and can be analyzed in the same way as above.

2. Ions

As in the He-Ar case, the He^+ count rate is very low, and small cross sections for this ionization in He-Kr and He-Xe collisions are thus expected. Also as in the previous case, both B' and C' (Fig. 8) are ascribed to simple ionization and He ionization with simultaneous Kr excitation, respectively. In the He-Xe case, the count rate is found to be so small that we are unable to study ionization leading to He^+ .

III. CROSS SECTIONS

A. He-Ne

Reduced cross sections $\rho(\tau)^1$ are presented in Fig. 9(a) and 9(b) for beam energies of 1 and 2 keV. The curve labeled S is the cross section obtained when *all* the scattered particles are counted, independent of charge state (neutral+ions) and of energy loss. At small values of $\tau = E\theta$, S behaves like A (elastic cross section). This is easily understood since for these very soft collisions no inelastic processes perturb the elastic cross section. We can then normalize (at small τ values) the experimental S and A cross sections to a theoretical estimate T , for purely classical elastic scattering from the ground-state potential $V(R)$. The $V(R)$ used here was calculated by Matcha and Nesbet⁸ for $R > 2$ bohr and is well fitted in this region by

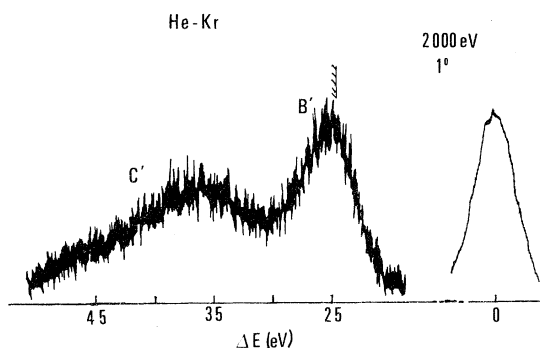


FIG. 8. Energy-loss spectrum of He^+ scattered from the He-Kr collision. The same labeling is used as in Fig. 2.

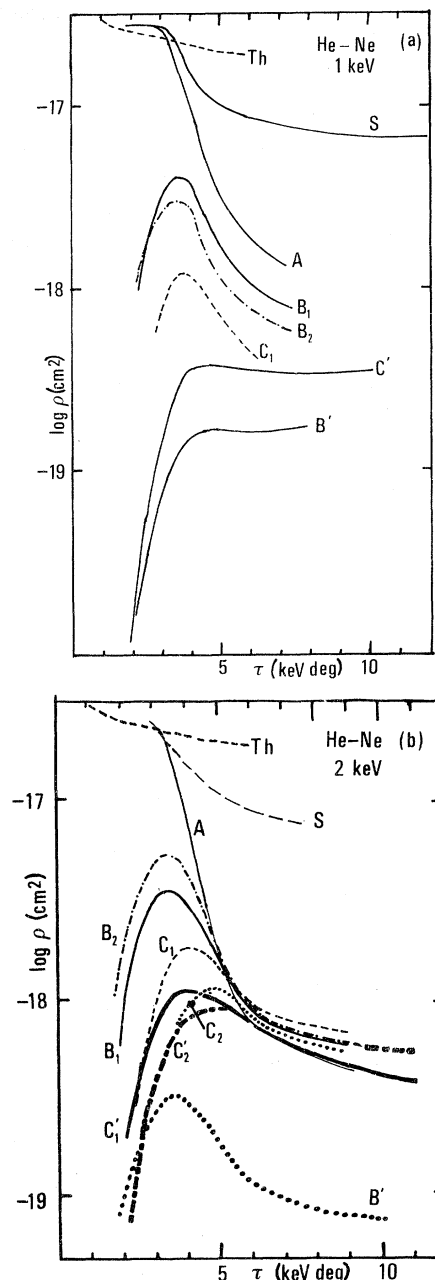


FIG. 9. Reduced differential cross sections [$\rho = \theta \sin\theta \sigma(\theta)$] as a function of the reduced angle ($\tau = E\theta$) for the He-Ne collision. (a) 1 keV: Th is the theoretical estimate for a purely elastic scattering (see text), S is the summed cross section (see text), A is the elastic cross section, B_1 and B_2 refer to one-electron excitation cross sections of Ne, and C_1 refers to simultaneous excitation of both He and Ne to the lowest levels. B' is the simple ionization cross section for He^+ production and C' is the cross section for $He^+ + Ne^*$ formation. (b) 2-keV data: The labeling is the same as in Fig. 9(a), in addition, C_2 refers to the simultaneous excitation of He and Ne on states higher than those labeled C_1 and C'_2 refers to the corresponding ionization process.

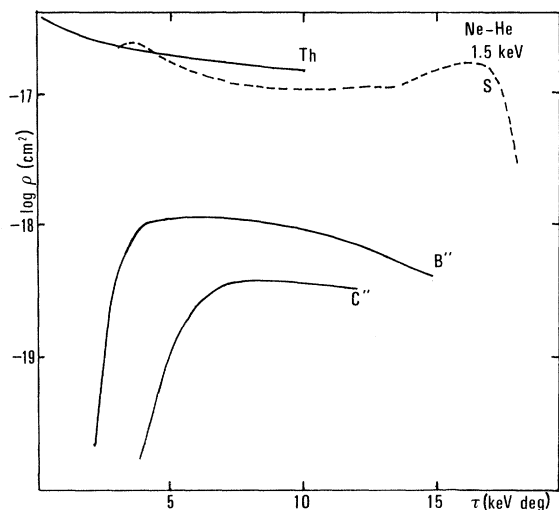


FIG. 10. Reduced differential cross sections for ionization producing Ne^+ at 1.5 keV. The same labeling is used as in Fig. 9. B'' and C'' refer, respectively, to simple Ne ionization and Ne ionization with simultaneous He excitation.

$$V(R) = 33.418e^{-2.322R} \text{ a.u.}$$

For $\tau > 4$ keV deg, A and even S drastically drop and T no longer has any physical meaning. This normalization procedure may lead to a large error which should affect only the *absolute* value of the cross section. The aim of this normalization is only to provide an estimation of the importance of the various processes.

Cross sections for B_1 and B_2 , corresponding to one-electron processes, behave similarly as a function of τ . They reach their maximum at $\tau \sim 3.6$ keV deg for all the impact energies. Only the relative intensity $\rho(B_2)/\rho(B_1)$ is energy sensitive.

The helium ionization cross section for B' has a maximum for the same τ value. This is especially clear at 2 keV [Fig. 9(b)]. At lower energy the maximum is followed by a plateau. It should also be pointed out that the cross section for B' is much smaller than the cross section for B_1 (Ne excitation).

The cross section for C_1 , corresponding to the

simultaneous one-electron excitation of both atoms to their first excited levels, presents a behavior similar to that of the B cross sections and has a maximum at a value of τ ($\tau \sim 3.8$ keV deg) slightly above the B maxima. Again C'_1 behaves as C_1 . In addition C'_2 (only given at 2 keV) and C_2 have the same shape and have a common maximum at a larger τ values ($\tau \sim 5$ keV deg).

Reduced cross sections for the ionization of the Ne from Ne + He collisions (processes B'' and C'') are presented in Fig. 10. The figure shows the marked dominance of the ionization of the neon as compared to the ionization of the helium. The ratio of these two cross sections at the same relative kinetic energy is about 70. This has to be related to the importance of neon excitation in the neutral reaction.

Integrating the experimentally obtained differential cross sections, we estimate the order of magnitude of the total cross section for several processes in Table I. The remarks made above on the selective excitation of Ne are of course reflected in the values of the total cross sections.

B. He-Ar

Cross sections at 1, 1.5, and 2 keV are given in Fig. 11. The absolute normalization is obtained as explained above. The elastic potential is taken from Matcha and Nesbet⁸ and is well fitted by

$$V = 31.395e^{-1.884R} \text{ for } R > 2.0 \text{ bohr.}$$

The elastic cross section A drops rapidly when the inelastic processes become important. Cross sections for B_1 and B_2 (one-electron excitation) attain their maximum values for $\tau \sim 2.5$ keV deg.

The two-electron excitation cross sections C are smaller than B and display a less-marked threshold dependence on the beam energy; ionization cross sections (B' and C') for He^+ production are measured at 1.5 keV and found to be *very small*, lying about two orders of magnitude below the Ar excitation cross sections. The angular dependence of both B' and C' is quite similar and resembles that of C . Estimates of total cross sections for several processes are also given in Table I.

TABLE I. Order of magnitude (in \AA^2) of total cross sections for some inelastic processes.

	He-Ne		He-Ar		He-Kr	
	1 keV	2 keV	1 keV	1.5 keV	1 keV	2 keV
Excitation B_1	0.2	0.2		0.4	1.1	1
B_2	0.15	0.25	0.55	0.8		
C	0.06	0.1		0.2	0.3	0.3
Ionization B'	0.015	0.02		0.002		
C'	0.03	0.08		0.007		10^{-3}

C. He-Kr, Xe

Cross sections for He-Kr collisions are given in Fig. 12. The normalization is obtained using an empirical potential derived from the He₂⁹ and Kr₂¹⁰ potentials using the combining rule proposed by Smith.⁹ In this way the following potential is obtained:

$$V = 53.9316 e^{-2.0982R}, \quad 1.6 < R < 3.1 \text{ a.u.},$$

$$V = 29.7752 e^{-1.806R}, \quad R > 3.1 \text{ a.u.}$$

The behavior of the cross sections is quite similar to the previous He-Ar case. We also note the major difference in the magnitude of the He ionization with respect to Kr excitation, a feature which becomes more marked as the atomic number of the rare-gas target increases.

The cross sections obtained at beam energies of 0.8, 1.5, and 2 keV for the He-Xe system are given in Fig. 13. The relative probability of two-electron transitions (C process) always remains very small as compared to that of the one-electron processes.

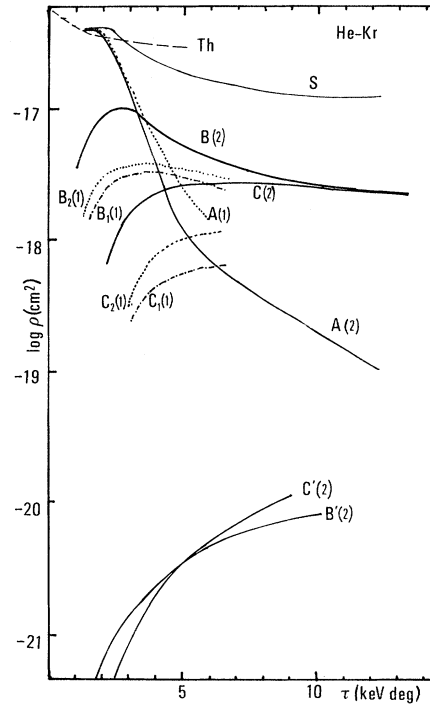


FIG. 12. Reduced differential cross sections for He-Kr. The labeling is the same as in Fig. 11.

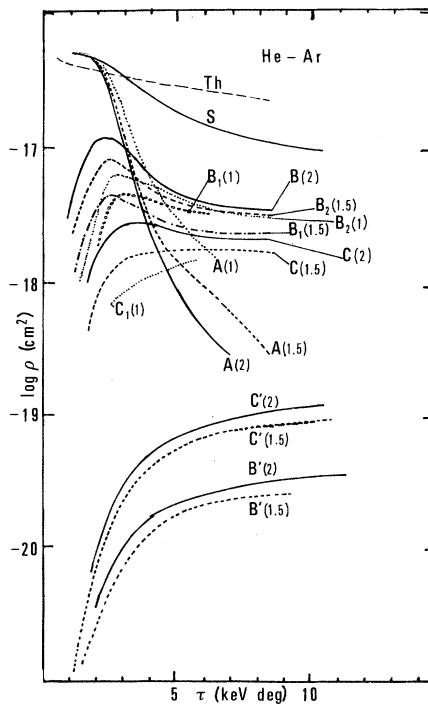


FIG. 11. Reduced differential cross sections for He-Ar collisions. The labeling is the same as in Fig. 9. Numbers in brackets designate the beam energy (in keV) at which the cross sections are determined.

IV. DISCUSSION

A. Helium-Neon

The diabatic correlation diagram (Fig. 14), constructed as proposed by Barat and Lichten³ for asymmetric systems, can serve as a starting point for a qualitative discussion of the experimental results.

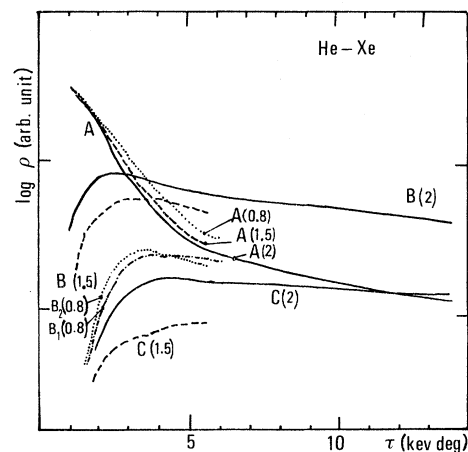


FIG. 13. Reduced differential cross sections for He-Xe collisions. The labeling is the same as in Fig. 11. Absolute ordinates are not estimated here.

In this picture an excitation process is thought to be induced only by one or two σ -electron transitions from the filled $3d\sigma$ MO to empty excited MO's. Since the $3d\sigma$ MO is correlated to the outer $2p_{\text{Ne}}\text{AO}$ (atomic orbital), excitation of the Neon atom is expected to be dominant.

For further discussion the corresponding diabatic diagram for the molecular states is needed. This diabatic diagram for many-electron states is shown in Fig. 15(a). Each of these states is described as a single electronic configuration of diabatic MO's (i.e., the independent electron model is assumed). The procedure then consists in correlating a particular state of the separated atoms ($R \rightarrow \infty$) with the appropriate state of the united atom ($R \rightarrow 0$) determined from the diabatic MO diagram. This is achieved by filling the diabatic MO's according to the Pauli principle.

The first diabatic MO crossing (Fig. 14) involves the excited $3s\sigma$ MO and should provide, by one- or two-electron transitions, the excitation of the following channels:

$$\text{He}(1s^2) + \text{Ne}(2p^5 3s), \quad \text{curve A};$$

$$\text{He}(1s^2) + \text{Ne}^*(2p^4 3s^2), \quad \text{curve C}.$$

The corresponding three-state crossings (X - C - A) are seen in Fig. 15a. The one-electron transition $3d\sigma$ - $3s\sigma$ is indeed seen to occur in small angle inelastic scattering (Fig. 9) and does lead to selective excitation of $\text{Ne}(2p^5 3s)$ (Fig. 1). Figure 15(a)

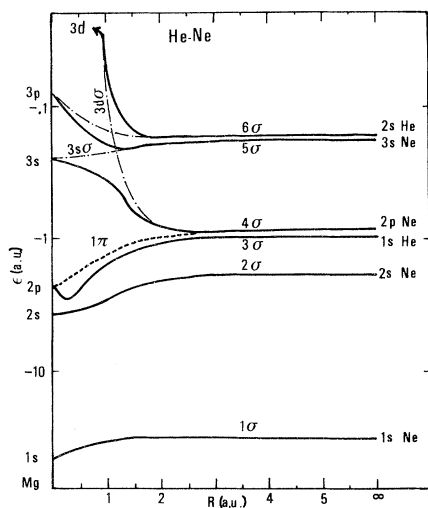


FIG. 14. MO correlation diagram for He-Ne. The shape of the adiabatic energy levels (full line: σ MO's; dashed line: π MO's) down to 1 a.u. is taken from previous (He-Ne) $^+$ calculations (Ref. 11 in text). The united atom limits are taken from Ref. 15. The predicted diabatic MO's from Ref. 3 (light dashed-dotted line) are labeled $3d\sigma$ and $3s\sigma$.

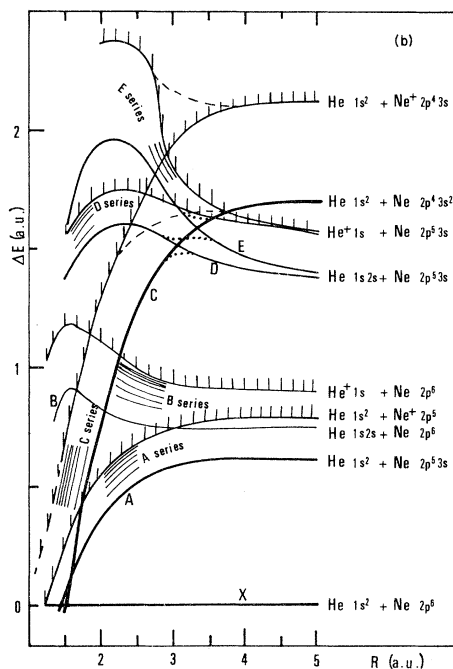
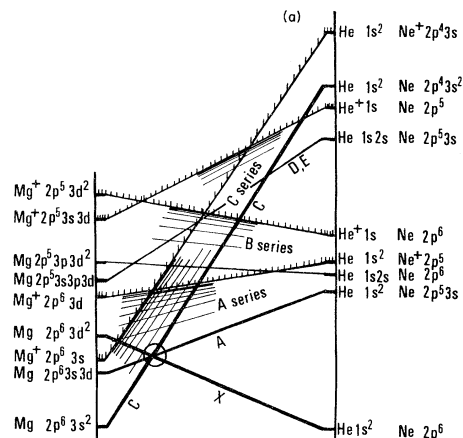


FIG. 15. (a) Schematic state-correlation diagram for He-Ne constructed from the diabatic MO correlation diagram of Fig. 14. (b) Potential energy curves for He-Ne ($^1\Sigma^+$) and (He-Ne) $^+$ ($^2\Sigma^+$) referred to the $X^1\Sigma^+$ state of He-Ne. These are obtained in the virtual orbital approximation using previous calculations on (He-Ne) $^+$ (Ref. 11). *A series*: dissociate into He + Ne*. The corresponding states have the configuration $(3\sigma^2 1\pi^4 4\sigma)_{\text{core}} n\sigma$, where $n > 4$. The continuum limit (shaded curve) of these series is the $X^2\Sigma^+$ ground state of He-Ne $^+$. *B series*: dissociate into He* + Ne. The corresponding configuration are $(3\sigma 1\pi^4 4\sigma^2)_{\text{core}} n\sigma$, where $n > 4$. *C series*: dissociate into He + Ne**. The corresponding configuration are $(3\sigma^2 1\pi^4)_{\text{core}} n\sigma n'\sigma$, $n = 5$, when $n' \geq 5$. *D and E series*: correspond to configuration $(3\sigma 1\pi^4 4\sigma)_{\text{core}} n\sigma n'\sigma$ and dissociate into He* + Ne*. The dotted and dashed lines show the effects of configuration interaction.

also shows that the $3d\sigma$ - $3s\sigma$ MO crossing leads to a large number of state crossings between the incoming X diabatic channel and states of the A series dissociating into $\text{He}(1s^2) + \text{Ne}(2p^5 nl)$. In addition the X state also crosses the infinite Rydberg C series, dissociating into $\text{He}(1s^2) + \text{Ne}(2p^4 3s nl)$. The crossings between the X incident channel and these two "crossed bands" (A and C series) constitute a typical pattern induced by a MO crossing. In particular this feature is encountered in closed-shell systems (see for example I). One- or two-electron transitions in this crowded region provide the primary mechanism for the observed inelastic scattering.

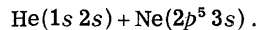
The predicted state diagram [Fig. 15(a)] is confirmed by the potential energy curves [Fig. 15(b)] estimated from previous $(\text{HeNe})^+$ calculations¹¹ using the virtual-orbital approximation. From this estimate, the location of the triple X - A - C crossing is found to be $R \approx 1.5$ bohr, and the multicrossing pattern arises in the range 1.2 bohr $\lesssim R \lesssim 1.5$ bohr.

Transitions to singly excited states of Ne and ground state of Ne^+ are then expected to be induced in the same narrow region, either directly or through couplings via the excited C state (see later discussion and discussion in I). Experimental findings, i.e., the similar behavior of the differential cross sections for all the single excitations of the Ne atom and the common position of the cross-section maxima ($\tau \approx 3.6$ keV deg.), are consistent with the estimated R_c value (1.5 bohr). As already mentioned, this mechanism should favor the $\text{Ne}(2p^5 3s)^1P$ level. That this is the case is apparent from the ratio of the peaks for the excitation of $\text{Ne}(2p^5 3s)$ and $\text{Ne}(2p^5 3p)$ (see Fig. 1).

The apparent dominance at certain energies of the B_2 peak is probably due to the overlap of several close-lying levels. Detailed information on these excitations could be obtained only by optical measurements. Single ionization of $\text{Ne}(B''$ in Fig. 3) is also found experimentally to be the dominant ionization process, in agreement with the above theoretical picture.

A comparison with the Ne-Ne case (I) shows a striking difference between symmetric and asymmetric collisions. Whereas the $3s$ level is dominant in He-Ne collisions, the same level is only weakly excited in the Ne-Ne case. This can be related to the proposed excitation mechanisms since the direct one-electron transition, $2p_{\text{Ne}} \rightarrow 3s_{\text{Ne}}$, is forbidden in the Ne-Ne case by the u - g symmetry ($4f\sigma_u$ - $3s\sigma_g$ crossing), while there are no such symmetries in the asymmetric He-Ne case. Two-electron transition ($2p_{\text{Ne}} \rightarrow 3s_{\text{Ne}}$) occurs in the same (X - A - C) region and should populate the $\text{Ne } 2p^4 3s^2$ autoionizing state (channel C on Fig. 15). Experi-

mental results are in apparent disagreement here since the first dominant two-electron process involves the simultaneous excitation of both particles,



However, the dependence of the corresponding C_1 cross section (Fig. 9) indicates that the same interaction region is concerned since the B_1 and C_1 cross sections behave in the same way. In addition, ejected-electron spectra⁵ do not show any peak corresponding to the autoionizing $\text{Ne}(2p^4 3s^2)$ states. Indeed, on the way out the C channel crosses molecular states dissociating in D and E and the associated Rydberg series. The effects of configuration interaction at the C - D and C - E crossings modify the single configuration curves, as shown by dotted lines in Fig. 15(b). This effect may account for the experimentally observed two-electron excitation processes.

Before reaching the C - D crossing the doubly excited C channel also crosses the complete Rydberg series B , dissociating into $\text{He}^* + \text{Ne}$ up to $\text{He}^+ + \text{Ne} + e^-$. (Note that the repulsive behavior of this series results from the creation of a vacancy in the inner and unpromoted $2p\sigma$ MO, i.e., 3σ on Fig. 14.) Such C - B crossings could then populate singly excited and ionized states of He. In fact, if we consider the states as having single MO configurations, $B(2p\sigma 3p\sigma 3d\sigma^2)$ and $C(2p\sigma^2 3s\sigma^2)$, they differ by three molecular spin orbitals and cannot be directly coupled. The experimental data, however, do not give direct evidence for the weakness of the helium excitation since the overlap of the excited levels of both atoms prevents a precise assignment to the observed B_2 peak. Nevertheless, the weakness of He excitation is clearly suggested by the ionization results. Figure 9(a) shows that the helium ionization (B') is smaller than both the neon excitation (B_1 or B_2) and ionization by more than one order of magnitude. The ionization limits of the D and E series correspond to the ionization of He with simultaneous Ne excitation in the lowest levels (C' in Fig. 9). Since the shape and the position of the maximum of the C' cross section is analogous to that of the C cross sections, the primary mechanism is thought to be common and again involves the interaction of C states with the corresponding D and E associated continua. The cross section is small since, as already discussed, the C , D , and E crossings are avoided.

Processes involved in C_2 and C'_2 cross sections require an interaction region at smaller internuclear distance where the high density of states considerably complicates a theoretical analysis. However, both C_2 and C'_2 are thought to have a common origin since their cross sections have the same

shape and the same angular behavior (Fig. 9). We believe that these processes involve either Rydberg states other than C itself, in the C series (for C_2 processes), or the associated continuum (for C'_2 processes).

It is interesting to compare the present results with those obtained for the isoelectronic (Li-Ne)⁺ system.¹² In both systems the primary excitation mechanism is identical: the spectra and cross sections for single-electron excitation of Ne are very similar. However, the (Li-Ne)⁺ C channel gives rise to Ne**(2p⁴3s²) since the corresponding (Li-Ne) D channel [Li⁺(1s 2s) + Ne(2p⁵3s)] now lies much higher than Ne**(2p⁴3s²) + Li⁺(1s²) and does not perturb the population of the C channel. This situation will be found again in the other He-rare-gas systems.

B. He-Ar

In this very asymmetric case, the "swapping"³ between the 1s_{He} and 2p AO's (atomic orbitals) causes the 1s_{He} to be promoted and correlated to the 3dσ_{Ca} orbital. The preferential excitation of He is thus *expected* from the resulting diabatic correlation diagram (Fig. 16). This is in complete disagreement with the experimental findings which show the almost exclusive excitation of Ar. Thus our ideas have to be revised. The experimental data suggest that the outer 3p_{Ar} electrons are promoted as in the He-Ne case. This corresponds to an avoided 3dσ-3pσ crossing (as shown by the 5σ and 6σ MO's in Fig. 16), at least for small relative velocity (~0.1 a.u.). The same situation will be met in the He-Kr and He-Xe systems. It should be pointed out that this gross failure in the applicability of the promotion model (correlation rules) to outer-shell problems occurs when an inner promoted MO crosses an outer filled MO. The necessary avoidance of such a crossing has the effect of promoting the outer MO. Further experimental evidence for this avoided crossing is found in the investigation of the ionic (He Ar)⁺ system where the same diabatic MO correlation diagram has to be used. The identical 3dσ-3pσ MO crossing should be reflected in the ionic system in a crossing between the molecular states dissociating into



The very small cross sections¹³ for the ground-state charge-exchange process ($\alpha \rightarrow \beta$) confirms the strong avoidance of the crossing.

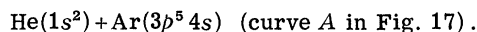
Another comparison can be made with the (Li Ar)⁺ system, which is isoelectronic with He-Ar. In this case the 1s_{Li}-3p_{Ar} crossing should also be avoided, thus leading to the 3p_{Ar} promotion. This

is confirmed experimentally by the absence of Li⁺ excitation.¹²

Actually the problem related to this "avoided" crossing is more complex, and even the existence of the crossing is questionable. Indeed, the only experimental evidence is the very low probability for electronic transitions between these MO's. In practice, one could first construct a diabatic correlation diagram using the "node-conservation rule."³ Then, assuming a large interaction at the crossing between an inner promoted MO and an outer filled MO., *the state diabatic correlation diagram is obtained by considering the promotion to involve the outer MO*, since the predicted MO crossing is no longer realistic.

This suggested new rule is of course valid for outer-shell excitation at moderate velocity (≤ 0.1 a.u.). Using this new correlation, the situation is now rather identical with the He-Ne case, and only the significant features are outlined.

The first active 3dσ-4sσ MO crossing leads by a one-electron transition to direct excitation of the channel



Of course, as in He-Ne, the entire Rydberg A series, including the continuum, is populated in the same region and accounts for the similar shapes of the corresponding differential cross sections.

A two-electron transition at the 3dσ-4sσ MO crossing gives rise to selective excitation of the C channel:

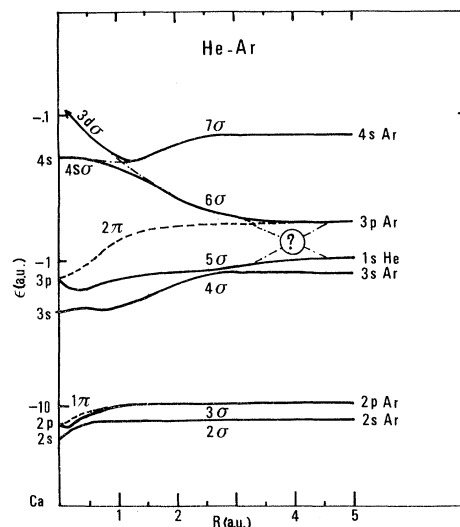


FIG. 16. MO correlation diagram for He-Ar. Same procedure and labeling as in Fig. 14. The problematic "crossing" (see text) 5σ-6σ is displayed with a question mark.

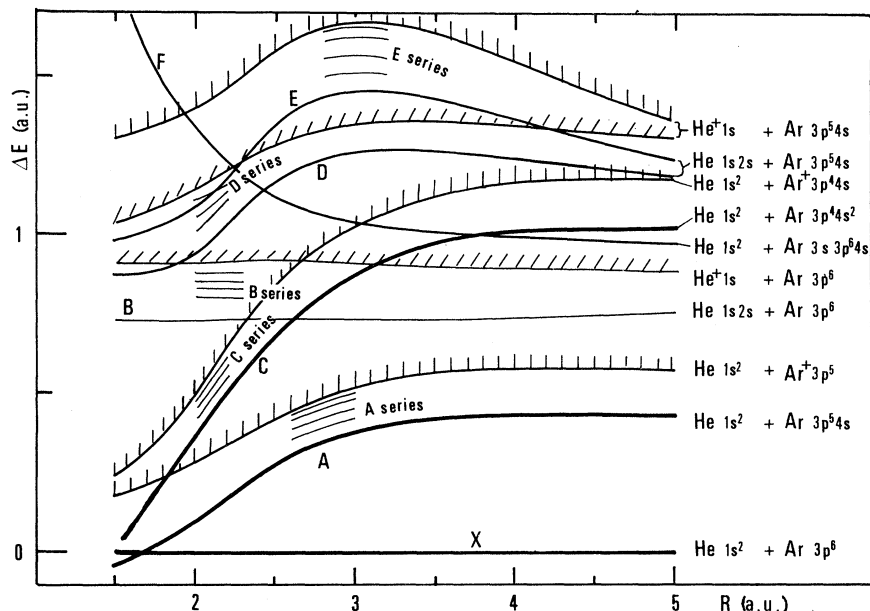
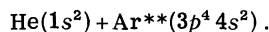


FIG. 17. Potential energy curves for He-Ar ($1\Sigma^+$) and (He-Ar) $^+$ ($2\Sigma^+$) referred to the $X^1\Sigma^+$ ground state of He-Ar. These are obtained in the virtual-orbital approximation using previous calculations (Ref. 16). As in Fig. 14. *A series*: $(5\sigma^2 2\pi^4 6\sigma)_{\text{core}} n\sigma \rightarrow \text{He} + \text{Ar}^*$; *B series*: $(5\sigma 2\pi^4 6\sigma^2)_{\text{core}} n\sigma \rightarrow \text{He}^* + \text{Ar}$; *C series*: $(5\sigma^2 2\pi^4)_{\text{core}} n\sigma n'\sigma \rightarrow \text{He} + \text{Ar}^*$; **D and E series*: $(5\sigma 2\pi^4 6\sigma)_{\text{core}} n\sigma n'\sigma \rightarrow \text{He}^* + \text{Ar}^*$; *F series*: $(4\sigma 5\sigma^2 2\pi^4 6\sigma)7\sigma \rightarrow \text{He} + \text{Ar} (3s 3p^6 4s)$.



Unlike the previous He-Ne case, the relative positions of the *C* and the *D*, *E* states, dissociating in $\text{He}^*(1s 2s) + \text{Ar}^*(3p^5 4s)$, are interchanged. Now, since the *C-D*, *E* crossings no longer exist only the *C* channel is populated. This is in agreement with experiment. Actually the $\text{Ar}(3p^4 4s^2)$ autoionizing configuration splits into three states (3P , 1D , and 1S) depending on the $\text{Ar}^{**}(3p^4)$ coupling scheme. Since in the molecular state involved (*C*) only the two $\sigma 3p$ (separate atom notation) electrons are excited, only the π^4 core dissociates into singlet states:

$$(\sqrt{2}^1D + ^1S)/\sqrt{3}.$$

This is indeed found in the experimental data where no 3P excitation is observed. The dominance of 1D is clearly demonstrated in Fig. 4. Furthermore, it is noteworthy that in contrast with the He-Ne case the ejected-electron spectra⁵ show autoionization states of argon. The latter spectra give evidence for the strong excitation of 1D (and perhaps 1S) autoionizing states.

As in the He-Ne case, the proposed mechanism does not allow for single-electron excitation or ionization in the helium since the appropriate molecular state (*B* in Fig. 17) cannot couple with the *C* channel (they differ by three spin orbitals). This is in agreement with the experiment, which does not present any evidence for helium excitation. Indeed in this He-Ar case, the peak assignment is made without any ambiguity since there is no overlap between the helium and argon excited levels. Moreover the measured simple-ionization

cross section is smaller than the argon-excitation cross section by more than two orders of magnitude.

Considering the possible excitation of $(3s 3p^6 nl)$ autoionizing levels of argon, only the lowest channel $(3s 3p^6 4s - F$ state in Fig. 17) can directly couple with the *C* channel, the higher-lying levels differing by three spin orbitals from *C*. The $\text{Ar}(3s 3p^6 4s)$ excitation is not observed in our energy-loss spectra because of the unfavorable signal-to-noise ratios, but it is clearly seen in the ejected-electron measurements.

Comparing the present results with those obtained for the isoelectronic $(\text{Li Ar})^+$ case,¹² one can note the similarities in the excited states involved. However, in $(\text{Li Ar})^+$ the inelastic processes have cross sections much smaller than those obtained in He-Ar since the MO promotion occurs at much smaller internuclear distance in the $(\text{Li Ar})^+$ system than in He-Ar. Indeed the crossing (or pseudocrossing) radius gets smaller as the promoted orbital lies deeper.

C. He-Kr and He-Xe

The He-Kr system is very similar to the He-Ar case. Again the $(4f\sigma - 4p\sigma)$ crossing affecting the He and outer MO's of Kr must be avoided, thus leading once again to the promotion of two σ electrons from the $4p_{\text{Kr}}$ shell. The single-electron transitions are similar to the two previous cases. However, as in the He-Ar system, two-electron transitions give rise mainly to doubly excited autoionizing states of Kr. The dominance of $4p^4 ^1D$ is also found in our energy-loss studies as well as

in the ejected-electron spectra⁵ and is explained in the same way. The same conclusions can be drawn for the He-Xe case.

V. CONCLUSION

Excitation and ionization processes in asymmetric He-rare-gas collision systems are investigated in the low-keV energy range. An important finding is the dramatic difference between the very weak excitation and ionization of the helium atom and that of the rare-gas partner.

The main features of the experimental results can be qualitatively understood in a quasimolecular framework. However, the interpretation requires a modification of the diabatic correlation rule in this particular energy range; in all these systems, we have to assume that only the *outermost filled orbital is promoted* and crosses empty MO's. This can be achieved by avoiding the crossings between $1s_{\text{He}}$ and $3p_{\text{Ar}}/4p_{\text{Kr}}/5p_{\text{Xe}}$ predicted by the usual diabatic correlation rules. Indeed, as experiment shows, these crossings are unrealistic. This is in fact not surprising since the conditions of applicability of the one-electron correlation rules³ are not fulfilled. In He-Ar for instance, the large subshell splitting in the $n=3$ AO levels of Ar is of the same order as the AO energies of $1s_{\text{He}}$ and $(3s, 3p)_{\text{Ar}}$. The same situation arises in the He-Kr, -Xe cases. In addition, preliminary results show that this also holds true in heavier systems such as Ne-Ar and Ne-Kr. In the He-Ne case this problem is not met since there is no $1s_{\text{He}}-2p_{\text{Ne}}$ crossing and the outer $2p_{\text{Ne}}$ orbital is promoted.

The problem related to the existence of a crossing between MO's arising from $1s_{\text{He}}$ and $3p_{\text{Ar}}/4p_{\text{Kr}}/5p_{\text{Xe}}$ is still not solved. A theoretical answer to this problem could be found by examining the wave functions of both orbitals to look for an interchange of their character. However, such a strongly avoided crossing will extend over a large range of internuclear distances, which would render a clear identification difficult.

In any case, when the shells begin to overlap the outermost MO of a closed-shell system is promoted (because of the Pauli exclusion principle and according to the new empirical rule). When the collision proceeds this MO becomes of the Rydberg type since it correlates to a Rydberg AO of the united atom. Crossings with high-lying empty Rydberg MO's (e.g., $\sigma 3s_{\text{Ne}}$ in the He-Ne

collision) are thus expected. In this case of Rydberg MO's, the applicability of the diabatic correlation rules is not questionable, as discussed in Ref. 3. In consequence the modification of the correlation rule only applies to the outermost crossings of outer filled orbitals.

The state correlation diagram constructed with these modified rules appears to be consistent with the experiments. In particular, the almost selective excitation and ionization of the heavier particle is well understood in this model.

As a general remark, it should be noted that the primary mechanism (i.e., one- or two-electron transitions at crossings of outer σ MO's with empty MO's) is common to all the rare-gas-rare-gas systems. However, in symmetric systems the $u-g$ symmetries may prevent direct population of the first excited "s" state, in contrast to their dominance in the asymmetric systems. One can also point out the relative decrease, for a given collision velocity, of the excitation probabilities as the asymmetry of the system increases. This is especially noticeable for two-electron transitions, which are very important in the symmetric systems as compared to asymmetric cases. The same behavior has already been observed in inner-shell excitation¹⁴ for the $2p$ promotion.

The He-Ne case differs from the others in the asymmetric systems in the two-electron process which involves simultaneous excitations in both collision partners instead of the excitation of auto-ionizing doubly excited states in the heavier systems (seen both in the energy-loss spectra and in ejected-electron spectra). This is well understood within the proposed model when one considers the relative position in the energy scale of both channels: The primary mechanism populates the molecular state leading to the double excitation of the heavier particle. *Only* in the He-Ne case does the channel corresponding to the simultaneous excitation of both particles lie below the doubly excited target channel, and it can therefore be populated. In particular, the present results show that triplet states can only be excited through two-electron transitions leading to simultaneous excitation of both particles. This is only the case for symmetric systems and for He-Ne. It is thus expected that, except for spin-dependent transitions, triplet excitations should be very weak in the other neutral rare-gas combinations. Optical measurements on such systems would provide a test of this conclusion.

*Permanent address: Department of Physics, University of Connecticut, Storrs, Conn. 06268.

†Equipe de recherche du C.N.R.S.

- ¹J. C. Brenot, D. Dhuicq, J. P. Gauyacq, J. Pommier, V. Sidis, M. Barat, and E. Pollack, *Phys. Rev. A* **11**, 1245 (1975).
- ²U. Fano and W. Lichten, *Phys. Rev. Lett.* **14**, 627 (1965).
- ³M. Barat and W. Lichten, *Phys. Rev. A* **6**, 211 (1972).
- ⁴J. C. Brenot, J. Pommier, D. Dhuicq, and M. Barat, *J. Phys. B* **8**, 448 (1975).
- ⁵G. Gerber, R. Morgenstern, and A. Niehaus, *J. Phys. B* **5**, 1336 (1972).
- ⁶M. Barat, D. Dhuicq, R. François, C. Lesech, and R. McCaroll, *J. Phys. B* **6**, 1206 (1973).
- ⁷E. Bolduc, J. J. Quémener, and P. Marmet, *J. Chem. Phys.* **57**, 1957 (1972).
- ⁸R. L. Matcha and R. K. Nesbet, *Phys. Rev.* **160**, 72 (1967).
- ⁹F. T. Smith, in *Proceedings of the Seventh International Conference on the Physics of Electronic and Atomic Collisions, Amsterdam, 1971*, edited by T. R. Govers and F. J. De Heer (North-Holland, Amsterdam, 1972), p. 1.
- ¹⁰V. I. Gaydaenko and V. K. Nikulin, *Chem. Phys. Lett.* **7**, 360 (1970).
- ¹¹V. Sidis and H. Lefebvre-Brion, *J. Phys. B* **4**, 1040 (1971).
- ¹²M. Barat, D. Dhuicq, R. François, and V. Sidis, *J. Phys. B* **6**, 2072 (1973).
- ¹³M. Barat, J. C. Brenot, J. Pommier, and V. Sidis (unpublished).
- ¹⁴B. Fastrup, G. Hermann, and K. J. Smith, *Phys. Rev. A* **3**, 1591 (1971).
- ¹⁵E. Clementi, *IBM J. Res. Dev.* **9**, 2 (1965).
- ¹⁶V. Sidis in Ref. 9, p. 120.